# Morphology, composition and mixing state of individual airborne particles collected after the 2017 Action Plan for the comprehensive control of air pollution in Beijing, China

Longyi Shao [1]*, Jie Li [1,2], Mengyuan Zhang [1], Yaowei Li [1], Tim Jones [4], Xiaolei Feng[1], Wenjun Li [1]

1 State Key Laboratory of Coal Resources and Safe Mining, College of Geoscience and Survey Engineering, China University of Mining and Technology (Beijing), Beijing 100083, China.

2 Beijing SDL Technology Co., Ltd. Beijing 102206, China

3 State Key Laboratory of Organic Geochemistry and Guangdong Key Laboratory of Environmental Protection and Resources Utilization, Guangzhou Institute of Geochemistry, Chinese Academy of Sciences, Guangzhou 510640, China

4 School of Earth and Environmental Sciences, Cardiff University, Museum Avenue, Cardiff CF10 3YE, UK

*Correspondence: ShaoL@cumtb.edu.cn

**Highlights:**

1. Individual airborne particles collected in Beijing after the Action Plan in 2017 were investigated.
2. Soot aggregates, organic, metal, mineral, fly ash, sulfate, and mixture particles were identified.
3. Sulfate particles and sulfate-mixed primary particles were dominant in Beijing air.
4. The relative percentages of sulfate, organic and soot aggregates increased after the action.
5. The contributions of vehicle emission and secondary reactions-increased.

**Abstract:** Beijing is one of several Chinese megacities with extremely serious air pollution-problems. In response to the air pollution ~~problem,~~ the central and municipal governments of China have implemented a series of actions; one of which is the "Action Plan for Comprehensive Prevention and Control of Autumn and Winter Air Pollution in Beijing-Tianjin-Hebei and Surrounding Areas 2017-2018" (the Action Plan) issued in 2017. The morphology, composition and mixing state of individual particles collected after the Action Plan was implemented were analyzed by transmission electron microscopy coupled with an energy-dispersive X-ray spectrometer (TEM-EDX). The relative percentages of different individual particle types and the main sources of the particulate pollutions before and after the Action Plan were compared. The results showed that sulfur was most frequently detected in the individual particles, and the particle types were mainly composed of soot aggregates, mineral particles, organic particles, metal particles, fly ashes, sulfate particles, and mixture particles. The mixture and sulfate particles dominated in the autumn samples, both for the haze and non-haze days. In winter the mineral and mixture particles dominated in samples from the non-haze days, while mixture particles and sulfate dominated in the samples from the haze days. The mixture particles in autumn were mainly the soot aggregates internally mixed with sulfate (S-soot type), while the mixture particles in winter were mainly the S-soot type and the mineral particles internally mixed with sulfate (S-mineral type). After the Action Plan, the relative percentages of sulfate particles, organic particles, and soot aggregates increased, while the relative percentages of

mineral particles, metal particles and fly ashes decreased. The contribution from coal-fired sources was reduced significantly as evidenced by the decrease in the fly ash particles. The vehicle emissions and secondary reaction of particulate matter became the main sources of atmospheric particulate matters as evidenced by increase in sulfate particles, organic particles, and soot aggregates.

## 1. **Introduction**

$PM_{2.5}$ (particles with aerodynamic diameters less than 2.5 μm) are dispersed in the atmosphere as solids or liquids, and they come from both natural sources as well as anthropogenic sources [*Huang et al.*, 2014b; *Zhang et al.*, 2017], causing a notable health risk [*Cao et al.*, 2012; *Shao et al.*, 2017a]. The Ambient Air Quality Standard of China (GB3095-2012) included the concentration limit of $PM_{2.5}$ in 2012. Since then the mass concentration of $PM_{2.5}$ has been incorporated into the atmospheric environmental quality assessment system. However, even though the $PM_{2.5}$ is now monitored, a large number of particles are still discharged into the atmosphere, with pollution levels well beyond the capacity of atmospheric circulation and dispersal. The large-scale haze events were still frequently occurring, especially when the meteorological conditions of lower atmosphere boundary layer, higher humidity, and temperature inversion are present [*Huang et al.*, 2014b; *Niu et al.*, 2015; *Rao et al.*, 2015; *Fu and Chen*, 2016; *Han et al.*, 2018; *Lu et al.*, 2018]. Severe air pollution episodes occurred frequently in Beijing, particularly in winter [*Wang et al.*, 2014a; *Wang et al.*, 2014b; *Sun et al.*, 2014; *Niu et al.*, 2016). With the very complex sources and evolution processes of aerosol

particles, air pollution control remained a great challenge in Beijing [*Sun et al.*, 2013], and the causes of haze episodes and rapid dispersion of airborne particles remained poorly understood [*Wang et al.*, 2016].

In order to minimize the frequent occurrences of atmospheric particulate pollution, the government of China introduced a series of pollution prevention and control measures from 2013 onwards, which have strengthened the controls on emissions from coal combustion, industrial activities, motor vehicles and surface fugitive dust~~ dust~~. One of these was the Air Pollution Prevention and Control Action Plan (APPCAP) issued on September 10, 2013 [*The State Council of China*, 2013]. The APPCAP is the first national strategy targeting $PM_{2.5}$ pollution and improving air quality in China by setting specific quantitative targets and clear time nodes [*Feng et al.*, 2019; *Li et al.*, 2020]. In particular, as a key city, the $PM_{2.5}$ concentration of Beijing should be kept below 60 $\mu g/m^3$ by 2017. To fulfill the target, Beijing Municipal Government made further efforts according to the guidance of the APPCAP, and has issued its own "Beijing 2013–2017 Clean Air Action Plan" (the Clean Air Action) in September 2013 [*PGBM*, 2013], which implemented much more stringent control measures than before. However, heavy pollution days still frequently occurred, with several cases of excessive increase of $PM_{2.5}$ during heavy pollution episodes in Beijing in December 2016 [*Zhong et al.*, 2017; *Wang et al.*, 2018; *Li et al.*, 2020]. Due to the frequent occurrences of serious atmospheric pollution by particulate matter in autumn and winter, the Chinese government issued the Action Plan for Comprehensive Prevention and Control of

Autumn and Winter Air Pollution in Beijing-Tianjin-Hebei and Surrounding Areas 2017-2018 (the Action Plan) [*MEPC,* 2017]. The main goal of the Action Plan was to fully meet the requirements of the Action Plan for Air Pollution Prevention and Control of 2013 [*Li et al.*, 2020]. Today the prevention and control of air pollution is of unprecedented concern, and with more comprehensive and strict coal-fired emission reduction measures the $PM_{2.5}$ annual concentrations in Beijing fell from 89.5μg/m$^3$ to 58μg/m$^3$ in just five years from 2013 to 2017 [*BEES*, 2018]. The air quality of Beijing is being consistently improved, with the steady growth in economic development including the GDP and total energy consumption [*UN Environment*, 2019].

In recent years, individual particle analysis using electron microscopy has been widely employed to characterize aerosol particles. Information on individual particles, such as the morphologies, elemental compositions, mixing states, and aging process, is important for understanding the particle formation and modeling the climate effects of atmospheric aerosols [*Pósfai and Buseck*, 2010; *Cappa et al.*, 2012; *Laskin et al.*, 2016; *Li et al.*, 2016a]. Several studies have used individual particle analysis to investigate the properties of aerosol particles in Beijing. For example, Wang et al. (2017) investigated the morphology and elemental composition of individual particles collected during haze days in Beijing, and observed that the high number percentages of sulfate particles (35.1%) were closely related to the air masses from adjacent areas south of Beijing where domestic coal combustion was commonplace [*Wang et al.*, 2017]. After the Action Plan, the pollution from domestic coal combustion have been

stringently controlled, and it is expected that to some extent the compositions of the individual particles will have changed. It is important to monitor the changes to the individual particles as a way to ground proof the effectiveness of the action plan in the reduction of coal combustion.

In this study individual particles from non-haze days and haze days in autumn and winter 2017 (after the Action Plan was implemented) were sampled. The morphology, composition, mixing state of these individual particles were investigated, and the main types of atmospheric particulate matter before and after the Action Plan were compared.

## 2. Materials and Methods

### 2.1 Sample Collection

The sampling location (116 °20′45.6”E, 39°59′37.1” N) was located at the China University of Mining and Technology (Beijing) in the northwestern Beijing, approximately 1 km from Beijing's north 4th Ring Road. The sampling site was surrounded by houses, streets, and shopping centers. The sampler was mounted on the roof of a campus building approximately 18 m above the ground. There were no major sources of industrial pollution in the area (Figure 1).

The samples of individual particles were collected under haze and non-haze conditions in autumn and winter after implementation of the Action Plan, 2017. A single-stage cascade impactor with a 0.5 mm diameter jet nozzle was used at a flow rate of 1.0 L / min. The particles were collected on copper TEM grids coated with carbon

film (carbon type-B, 300-mesh copper, Tianld Co., Beijing, China). For particles with an aerodynamic diameter of 0.25 μm and a density of 2 g/cm$^3$, the collection efficiency of the impactor is 50%. Sampling duration varied from 30–60 seconds depending on the concentration of $PM_{2.5,}$ which was determined from other sources . The Kestrel 5500 Pocket Weather Tracker (Nielsen-Kellerman Inc., Minneapolis, MN, USA) was used to measure relative humidity, atmospheric pressure and ambient temperature (Table 1). After collection, the samples were placed in a desiccator at 25 ± 5 °C and 20 ± 3% RH to prevent contamination by ambient air.

**2.2 Experimental**

Individual particles were characterized using a transmission electron microscope (TEM) equipped with an energy-dispersive X-ray spectrometer (EDX). The particles on the copper TEM grids were viewed under a Hitachi H-8100 TEM (Hitachi, Ltd., Tokyo, Japan). The TEM was operated with an acceleration voltage of 300 kV. The particles were normally heterogeneously distributed on the TEM grids with coarser particles near the center and the finer particles towards the periphery. To guarantee that the analyzed particles were representative of the whole size range, 3–4 areas were chosen from the center and periphery on each grid. All individual particles larger than 0.1 μm in the selected areas were analyzed. Elemental compositions were determined semi-quantitatively using ~~an~~ EDX. In order to determine the element composition characteristics of aerosol particles in the sampling period, the EDX was applied to each

particle in the selected squares. A low current and small beam spot were used to avoid adverse effect from the electron beam on the particles. Copper was not considered in the analysis because of interference from the copper TEM grid [*Li and Shao*, 2009; *Shao et al.*, 2017b].

## 3. Results and discussion

### 3.1. Element frequency in the analyzed particles

The individual particles in Beijing often showed complex compositions, with more than 17 elements being detected by EDX. In addition to C and O which were detected in all the particles, N, Na, Mg, Al, Si, P, S, Cl, K, Ca, Ti, Mn, Fe, Zn, and Cr were detected in 1731 analyzed particles (Figure 2). It can be seen that sulfur had the highest detection frequency which was detected in more than 85% of the particles, followed by Si (>65%), K (>55%), Al (>50%), N (>40%), Na (>35%), Mg (>30%), Fe (>25%), Ca (>15%), Zn (>7%) and Cl (>7%). P and heavy metals (e.g., Mn, Ti, and Cr) were present in less than 5% of the analyzed particles.

Figure 3 showed the detection frequency of these 17 elements in individual particles under different meteorological conditions in autumn and winter. For the autumn samples, Na, S, Cl and Zn were mostly detected in the haze days, and Mg, Al, Si, K, Ca, Ti, Mn and Fe were mostly detected in the non-haze days. For the winter samples, Na, Mg, Al, Si, S, Cl, K, Ca, Mn and Zn were mostly detected in the haze days, and the Ti and Fe were mostly detected in the non-haze days.

S and N are major elements in sulfate and nitrate, and are often regarded as the products of secondary chemical reaction in the atmosphere [*Li et al.*, 2016a]. The detection frequency of S and N was high in both autumn and winter, with values being higher in the haze day than in the non-haze days. This suggests that $PM_{2.5}$ levels were seriously affected by secondary chemical reactions or secondary transformation of primary particles after the Action Plan. The rapid generation of secondary inorganic components such as S and N may have promoted the significant growth of $PM_{2.5}$ and accelerated the formation of haze weather [*Huang et al.*, 2014b; *Fu and Chen*, 2016].

The detection frequencies of Mg, Al, Si, K, Ca and Mn showed different trends in autumn and winter, with the higher values being in the non-haze days of autumn, and in the haze days of winter. As these elements are the main components of crustal mineral particles [*Song et al.*, 2014], their high detection frequencies in the winter haze days indicated that during winter, the $PM_{2.5}$ in Beijing was seriously affected by surface dust. Under the meteorological conditions of high humidity and temperature inversion, the contribution of the mineral particles suspended from the surface dust such as road and construction dust, and unvegetated lands in winter was higher in winter than in autumn. The high detection frequencies of these elements in the autumn non-haze days implied that during autumn, the non-haze days with lower humidity, compared with the haze days with higher humidity, may favor the accumulation of these elements.

### 3.2 Major types of individual particles

According to the results from the TEM-EDX analyses, all the analyzed particles were classified into seven types; soot aggregates, organic, metal, mineral, fly ash, sulfate, and mixture particles (Table 2).

Soot aggregates, also known as black carbon (BC) or elemental carbon (EC), are chain-shaped aggregates containing spherical carbon particles with sizes ranging from 10 to 100 nm [*Li et al.*, 2016a]. The chain-like, cluster-like, and compact-like morphology of soot aggregates were extremely stable under the electron beams (Figure 4a, b, c). Soot aggregates came mainly from vehicles emissions from burning fossil fuel [*Xing et al.*, 2018; *Xing et al.*, 2017]. The main elements in the soot aggregates were C, but also contains minor O, Si and K.

Mineral particles had irregular shapes and were extremely stable and non-volatile under strong electron beams (Figure 4d, e, f). They mainly originated from dusts such as construction and road dust. Some mineral particles are believed to be sourced from the long-distance transport of dust storm material, and had larger particle sizes than 2 μm [*Li et al.*, 2018]. The main components of mineral particles were crustal elements such as Si, Al, Ca and Fe. There are a large number of silica-aluminate minerals (Si, Al) among them, and $CaSO_4$, Ca-rich, and other mineral particles were also found.

Organic particles included primary organic particles (POM) and secondary organic particles (SOM). Primary organic particles were spherical or nearly spherical and extremely stable under the electron beams (Figure 4g), being mainly sourced from the

212 combustion of fossil fuels and biomass [*China et al.*, 2013; *Liu et al.*, 2017]. The
213 morphology of secondary organic particles was irregular, and most of them were
214 internally mixed with secondary sulfate particles (Figure 4h). They were mainly formed
215 by the oxidation of organic matter in the gas phase in the atmosphere [*Huang et al.*,
216 2014b]. Under the electron beams, the secondary organic particles were observed to
217 rapidly volatilize [*Hou et al.*, 2018a].

218 The metal particles had spherical and irregular shapes, with the Fe-rich particles
219 being most abundant, followed by Mn-rich and Zn-rich particles (Figure 4i, j, k). These
220 metal particles came mainly from the emissions of heavy industry and the combustion
221 of waste, biomass, and fossil fuels [*Gaston et al.*, 2013].

222 The fly ashes displayed a spherical morphology, mainly containing Si and Fe, with
223 occasionally a small amount of Ca, Ti, Mn and Al (Figure 4l). The fly ashes with small
224 particle sizes were mostly mixed with secondary particles such as sulfates to form
225 composite particles, and rarely exist on their own. They were mainly sourced from the
226 combustion of coal [*Hou et al.*, 2018b; *Wang et al.*, 2019].

227 The sulfates consisting of ammonia sulfate, potassium sulfate, and sodium sulfate
228 were irregular or round in shape, and easily volatilized under the electron beam (Figure
229 4m, n, o, p). These sulfate particles had a 'foam-like' morphology after volatilizing
230 under the beam, and they mostly presented a core-shell structure. Previous studies had
231 shown that the cores were sulfates such as sodium sulfate and potassium sulfate, while
232 the outer shell were organic matter [*Li et al.*, 2016b].

233 The mixture (composite) particles were sulfate particles mixed with primary
234 particles, with a few mixture particles as mineral particles internally mixed with nitrate.
235 The mixture particles showed an irregular shape and core-shell structure under the TEM.
236 The mixture particles can be further divided into six different sub-types including: the
237 soot aggregates internally mixed with sulfate (S-soot); the metal internally mixed with
238 sulfate (S-metal); the fly ash internally mixed with sulfate (S-fly ash); the mineral
239 particles internally mixed with sulfate (S-mineral); the primary organic particles
240 internally mixed with sulfate (S-POM); and the mineral particles internally mixed with
241 nitrate (N-mineral) (Table 2).

242 Nanoscale soot and fly ash particles were bonded to the surface or interior of the
243 sulfate particles in the S-soot and S-fly ash particles. There were some core-shell sulfate
244 particles in which the outer organic matter covered the soot aggregates and fly ashes
245 (Figure 5a, b). The metal particles were mostly Mn-rich, Fe-rich, and Zn-rich particles,
246 and internally mixed with sulfate particles in the S-metal particles (Figure 5d). Primary
247 organic particles and mineral particles were mostly adsorbed on the surface of sulfate
248 particles in the S-POM and S-mineral particles (Figure 5e, f). Some mineral particles,
249 which were dominated by alkaline minerals, tended to stick onto the surface of sulfate
250 particles. N-mineral particles were nitrate coatings on alkaline mineral particles (Figure
251 5c) [*Li*, 2009].

252 **3.3 The relative abundance of individual particles**

253 ***3.3.1 Overall relative abundance of different types of individual particles***

254 The relative abundance of different types of individual particles collected in haze
255 days and non-haze days after the Action Plan was calculated. A total of 1731 individual
256 particles were analyzed that including 862 particles for the autumn non-haze days and
257 520 particles for autumn haze days, 146 particles for winter non-haze days and 203
258 particles for winter haze days (Figure 6).

259 Overall, the sulfate and mixture particles were the highest percentage of the 1731
260 particles, accounting for 44.66% and 39.11% respectively, this was followed by soot
261 aggregates (4.91%), mineral particles (4.27%), primary organic particles (3.06%),
262 secondary organic particles (2.31%), metal particles (1.27%) and fly ashes (0.4%). As
263 the sulfate and mixture particles were closely associated with atmospheric secondary
264 chemical reactions, the results showed that these secondary chemical reactions
265 generated the major contributions of the airborne particles after the 2017 Action Plan.

266 ***3.3.2 Comparison of particle types for haze and non-haze days in autumn***

267 In the autumn non-haze days, the sulfate particles were the highest percentage of
268 all analyzed particles, accounting for 64.8%, followed by mixture particles (31.3%),
269 soot aggregates (2.2%), primary organic particles (0.6%), secondary organic particles
270 (0.5%), metal particles (0.3%) and mineral particles (0.2%) in descending order. Fly
271 ashes were not found in the samples collected in the autumn non-haze days.

272 In the autumn haze days, the percentage of mixture particles was the highest at

50.0%, followed by sulfates particles (25.4%), soot aggregates (6.9%), secondary organic particles (6.3%), mineral particles (4.6%), primary organic particles (3.7%), metal particles (2.7%) and fly ashes (0.4).

It can be seen (Figure 6) that the percentages of sulfate and mixture particles were significantly higher than other particles in both haze and non-haze days in autumn. In addition in autumn, the percentage of the sulfate particles in the non-haze days was significantly higher than in the non-haze days, while the percentage of mixture particles in haze days was significantly higher than that in the non-haze days. The percentages of soot aggregates, organic particles, metal particles, mineral particles and fly ash in haze days were relatively elevated at various degrees compared with non-haze days. The results showed that sulfate particles were easily mixed with other primary particles by heterogeneous chemical reactions in the liquid phase during haze days when a large number of primary particles accumulated [*Wang et al.*, 2017; *Li et al.*, 2017a]. A large number of mixture particles were generated during the aging process of sulfate particles [*Yuan et al.*, 2015; *Wang et al.*, 2016].

***3.3.3 Comparison of particle types for haze and non-haze days in winter***

In the winter non-haze days, the mixture and mineral particles had the highest percentages at 26.7% and 26.0% respectively, followed by primary organic particles (15.8%), soot aggregates (14.4%), sulfate particles (13.7%), metal particles (2.1%), and fly ashes (1.4%). Secondary organic particles were not found in the samples of the winter non-haze days.

In the winter haze days, the mixture and sulfate particles had the highest percentages at 53.2% and 30.5% respectively, followed by mineral particles (4.9%), soot aggregates (4.4%), primary organic particles (3.0%), secondary organic particles (1.5%), fly ashes (1.5%) and metal particles (1.0%).

It can be seen (Figure 6) that the winter samples of the non-haze days were dominated by mineral and mixture particles, while the samples of the haze days were dominated by sulfate and mixture particles. The results showed that the dust sources made a higher contribution to the percentage of mineral particles in winter, because of the frequent windy weather and low humidity in the non-haze days. However, the high humidity and less windy conditions of haze weather favored the generation of secondary particles and the hygroscopic growth of primary particles [*Sun et al.*, 2018], which would increase the relative percentage of sulfate particles [*Qi et al.*, 2014] and other particles internally mixed with sulfate particles increased significantly [*Li et al.*, 2014; *Wang et al.*, 2017]. As a result, the haze day samples had significantly higher percentages of sulfate and mixture particles compared with the non-haze days. In addition, compared with non-haze conditions, the haze day samples had an increased percentage of mixture particles, sulfate particles, and secondary organic particles, and a decreased number percentage of mineral particles, primary organic particles, soot aggregates and metal particles. The result showed that the primary particles were more readily transformed into secondary particles such as sulfate and mixture particles in haze days, which resulted in the decreased percentage of primary organic particles and

315 the increased percentage of the secondary organic particles. Previous studies [*Li et al.*,
316 2016a; *Wang et al.*, 2017] have shown that the surface of mineral particles was a good
317 substrate for heterogeneous chemical reactions with $SO_2$ and acidic gases to generate
318 sulfates; while soot aggregates, primary organic particles, and metal particles were
319 easily adsorbed on the surface of sulfate particles and mixed with sulfates through
320 complex chemical reactions.

321 ***3.3.4 Comparison of abundance of secondary particles (sulfate particles and***
322 ***mixture particles) for the non-haze days in autumn and winter***

323 The comparisons between the percentage of particle types under different
324 meteorological conditions shows that the secondary particles (sulfate particles and
325 mixture particles) were dominant in both haze and non-haze days in winter and autumn.
326 For the non-haze samples, the percentage of sulfate particles and mixture particles in
327 autumn was higher than that in winter, and the percentages of mineral particles, POM
328 and soot aggregates in winter were also higher than those in autumn. These results
329 indicate that the non-haze days in autumn are more likely to generate secondary
330 particles when compared to the non-haze days in winter. There was a significant number
331 of mineral dust particles in winter non-haze days due to the low humidity and the windy
332 weather. It is noted that some rural areas around Beijing still used traditional heating
333 methods such as burning coal and wood, which would emit a large amount of primary
334 organic particles (POM) [*Li et al*., 2016b].

335 For the haze samples, the relative percentage of sulfate and mixture particles was

slightly higher in winter than in autumn, and the other particles are mostly lower in winter than in autumn. The results showed that secondary chemical reactions were more prevalent during the winter haze than during the autumn haze. During winter heating periods, more coal emissions from the countryside around Beijing might contribute more $SO_2$ and acidic gases [*Wang et al*., 2017] which would favor the generation of sulfates and mixture particles under the high humidity haze weather [*Li and Shao*, 2009; *Wang et al.*, 2017].

### *3.3.5 Comparison of abundance of sub-types of the mixture particles for haze and non-haze days in autumn and winter*

The percentages of mixture particles in both non-haze days and haze days were relatively high, and the values for the haze days was significantly higher than the non-haze days. According to the major elemental compositions, the mixture particles can be sub-divided further into six sub-types, including S-soot, S-mineral, S-POM, S-metal particles, S-fly ash and N-mineral particles (Table 2).

A statistical analysis was undertaken for these different sub-types of mixture particles for the haze and non-haze day of autumn and winter (Figure 7). In the autumn non-haze days, the percentage of the S-soot particles was the highest and reached 78.1%, followed by S-mineral particles (8.9%), S-POM particles (7.0%), S-metal particles (3.3%), S-fly ash (2.2%) and N-mineral (0.4%). In the autumn haze days, the S-soot particles were the highest percentages of all analyzed particles, at 83.8%, followed by S-mineral particles (5.8%), S-fly ash (5.4%), S-metal (3.5%) and N-mineral (1.5%). S-

POM particles were not found in the samples collected in the autumn haze days. In the winter non-haze days, the percentage of S-mineral and S-soot particles were the highest and reached 46.2% and 43.6%, respectively, followed by S-fly ash (5.1%), S-metal and S-POM particles (2.6%). N-mineral particles were not found in the samples collected in the winter non-haze days. In the winter haze days, S-soot and S-mineral particles were the highest percentages of all analyzed mixture particles, at 46.3% and 33.3%, respectively, followed by S-POM particles (13.9%), S-metal particles (4.6%) and S-fly ash (1.9%). N-mineral particles were not found in the samples collected in the winter haze days.

The comparison of the percentage of mixture particles under haze and non-haze conditions in autumn and winter demonstrated a number of interesting atmospheric phenomena. The mixture particles in autumn were mainly S-soot, accounting for 80%, whereas the mixture particles in winter were mainly S-soot and S-mineral, accounting for 80%-90%. These results indicate that the ambient atmosphere of Beijing in autumn and winter were seriously affected by vehicle emissions [*Li et al.*, 2020]. Motor vehicles emitted large amounts of soot aggregates, which could be internally mixed with sulfate particles by complex chemical reactions in the atmosphere [*Li et al.*, 2017b; *Xing et al.*, 2020]. In addition, the percentage of S-mineral particles significantly increased in winter compared with autumn. In a similar fashion the percentage of S-POM increased in winter haze days. The results indicated that the ambient atmosphere of Beijing in autumn was seriously affected by vehicle emissions, while the ambient atmosphere in

winter was affected by dust and coal emissions from surrounding areas in addition to vehicle emission. Due to the prevailing northwesterly wind in winter non-haze days a large number of mineral particles re-suspended from road dust, building dust and other pollution sources by the high winds can internally mix with sulfates through heterogeneous chemicals reactions in the atmosphere. These mineral particles suspended in the atmosphere during non-haze days would facilitate the internal mixing with sulfates [*Li et al.*, 2018; *Okada et al.*, 2005], resulting in a noticeable increase in the percentage of S-mineral particles in winter. In addition, in some rural areas around Beijing, coal is still used for heating in winter 2017, and the stable meteorological conditions and high humidity in haze days would promote the mixing of the POM emitted from coal-combustion with the sulfates by heterogeneous chemical reactions.

### 3.4 A comparison with the individual particles before the Action Plan

In order to understand the changes of individual particle compositions based on TEM-EDX after the Action Plan, the results were compared with the data of autumn and winter of 2013, which represented the stage before the Action Plan. The data on $PM_{2.5}$ concentrations were obtained from The U.S. Embassy Air Quality Online Monitoring and Analysis Platform (http://www.young-0.com/airquality/). It can be seen from Figure 8 that the concentration of $PM_{2.5}$ in Beijing decreased significantly in autumn and winter after the Action Plan.

Figure 9 shows the percentages of different types of individual particles during

haze days in autumn and winter before and after the Action Plan. The percentages of each type of individual particles in autumn before the Action Plan showed that the percentages of sulfate and mineral particles were higher, at 32.78% and 27.79%, respectively, followed by metal (14.96%), fly ash (13.54%), soot aggregates (5.70%), organic particles (5.23%) (Guo, 2015). The percentages of each type of individual particles in autumn after the Action Plan showed that sulfate and organic particles became the dominant type at 50.77% and 20.00% respectively, followed by soot aggregates (13.85%), mineral (9.23%), metal (5.38%), fly ash (0.77%). The percentages of each type of individual particles in winter before the Action Plan showed that sulfate particles had the highest value, being 29.29%, followed by mineral (21.89%), metal (17.46%), fly ash (16.86%), soot aggregates (7.69%) and organic particles (6.80%). The percentages of each type of individual particles in winter after the Action Plan showed that the sulfate particle remained highest at 65.26%, followed by mineral (10.53%), organic particles and soot aggregates (9.47%), fly ash (3.16%), and metal particles (2.11%).

By comparing the percentage of each type of individual particle in haze days before and after the Action Plan the percentages of sulfate particles, organic particles, and soot aggregates increased, while the percentage of mineral particles, metal particles and fly ash particles decreased significantly in the autumn and winter haze episodes.

These results indicated that after the Action Plan (especially the coal-burning ban), primary particles such as fly ash and metal particles emitted from coal-burning were

419 significantly reduced, while organic particles and soot aggregates emitted from vehicle
420 emissions became the main primary particles. In addition, secondary particles such as
421 sulfate became the main component of $PM_{2.5}$ in autumn and winter, and the secondary
422 conversion of primary particles had become the main source of $PM_{2.5}$ in the ambient
423 atmosphere of Beijing. Considering the very efficient control on the coal-burning
424 emissions and relatively less vigorous control of vehicle emission (*Li et al.*, 2020),
425 vehicle emissions and related secondary chemical reaction particles, which contribute
426 the relative high percentages of sulfate, organic and soot aggregate particles, requires
427 further emissions control.

428 **4 Conclusions**

429 Seventeen elements; C, O, N, Na, Mg, Al, Si, P, S, Cl, K, Ca, Ti, Mn, Fe, Zn, and
430 Cr were detected in a total of 1731 individual airborne particles collected in Beijing
431 after implementation of the 2017 Action Plan. With the exception of C and O, the
432 detection frequency of S was the highest among all detected elements in both non-haze
433 days and haze days. The detection frequency of Mg, Al, Si, K, Ca, and Mn were higher
434 in non-haze days than haze days in autumn, with the reverse occurred in winter with
435 values were higher in haze days than non-haze days.

436 Soot aggregates, organic, metal, mineral, fly ash, sulfate, and mixture particles
437 were identified in $PM_{2.5}$ collected in non-haze days and haze days in autumn and winter
438 after the Action Plan in Beijing. Mixture particles and sulfate particles dominated in
439 autumn non-haze days and haze days. Mineral particles and mixture particles were

dominant in the winter non-haze days, while mixture particles and sulfate particles were dominant in the winter haze days.

The mixture particles under different meteorological conditions in autumn and winter in Beijing displayed different mixing states. The S-soot, S-metal, S-fly ash, S-mineral, S-POM and N-mineral were identified in mixture particles, with the S-soot being mainly present in autumn, and the S-soot and S-mineral being mainly present in winter.

After implementation of the Action Plan, percentages of sulfate particles, organic particles, and soot aggregates increased in both autumn and winter, while the relative percentages of mineral particles, metal particles and fly ash particles decreased. The contribution of coal-burning sources to the atmosphere was significantly reduced, and motor vehicle emissions and secondary reactions particulates became the main sources of atmospheric particulate pollution.

**Acknowledgments**

This study is supported by the National Natural Science Foundation of China (Grant No. 42075107), the Projects of International Cooperation and Exchanges NSFC (Grant No. 41571130031) and the Yueqi Scholar fund of China University of Mining and Technology (Beijing).

# Reference


BEES (Beijing Ecology and Environment Statement), (2018). available at. http://sthjj.beijing.gov.cn/bjhrb/zrqskqzl/849908/index.html. (in Chinese).

PGBM (The People's Government of Beijing Municipality), (2013). Beijing 2013–2017 Clean Air Action Plan. http://www.beijing.gov.cn/zhengce/zfwj/zfwj/szfwj/201905/t20190523_72673.html (accessed 12 September 2013). (in Chinese).

Boyd, P. W., and Ellwood, M. J. (2010). The biogeochemical cycle of iron in the ocean, *Nature Geoscience*, *3*(10), 675-682.

Cao, J., Xu, H., Xu, Q., Chen, B., and Kan, H. (2012). Fine particulate matter constituents and cardiopulmonary mortality in a heavily polluted Chinese city, *Environmental Health Perspectives*, *120*(3), 373-378.

Cappa, C. D., Onasch, T. B., Massoli, P., Worsnop, D. R., Bates, T. S., Cross, E. S. et al. (2012). Radiative absorption enhancements due to the mixing state of atmospheric black carbon, *Science, 337(6098):*1078.

China, S., Mazzoleni, C., Gorkowski, K., Aiken, A. C., and Dubey, M. K. (2013). Morphology and mixing state of individual freshly emitted wildfire carbonaceous particles, *Nature Communications*, *4*(7), 2122.

Feingold, G., Mccomiskey, A., Yamaguchi, T., Johnson, J. S., Carslaw, K. S., and Schmidt, K. S. (2016). New approaches to quantifying aerosol influence on the cloud radiative effect, *Proceedings of the National Academy of Sciences of the United States of America*, *113*(21), 5812.

Feng, Y., Ning, M., Lei, Y., Sun, Y., Liu, W., Wang, J. (2019). Defending blue sky in China: Effectiveness of the “Air Pollution Prevention and Control Action Plan” on air quality improvements from 2013 to 2017. *Journal of Environmental Management. 252*:109603. https://doi.org/10.1016/j.jenvman.2019.109603.

Fu, H., and Chen, J. (2016). Formation, features and controlling strategies of severe haze-fog pollutions in China, *Science of the Total Environment*, *578*, 121.

Gaston, C. J., Quinn, P. K., Bates, T. S., Gilman, J. B., Bon, D. M., Kuster, W. C., and

Prather, K. A. (2013). The impact of shipping, agricultural, and urban emissions on single particle chemistry observed aboard the R/V Atlantis during CalNex, *Journal of Geophysical Research Atmospheres*, *118*(10), 5003-5017.

Georgakakou, S., Gourgoulianis, K., Daniil, Z., and Bontozoglou, V. (2016). Prediction of particle deposition in the lungs based on simple modeling of alveolar mixing, *Respiratory Physiology & Neurobiology*, *225*, 8-18.

Guo Menglong, 2015, Physico-chemical properties of the PM2.5 in ambient air of Beijing during heavily polluted periods. MSc thesis of China University of Mining and Technology (Beijing). 1-66pp. (in Chinese with English abstract)

Han, S., Liu, J., Hao, T., Zhang, Y., Li, P., Yang, J., Wang, Q., Cai, Z., Yao, Q., and Zhang, M. (2018). Boundary layer structure and scavenging effect during a typical winter haze-fog episode in a core city of BTH region, China, *Atmospheric Environment*, *179*.

Hou, C., Shao, L., Hu, W., Zhang, D., Zhao, C., Xing, J., Huang, X., and Hu, M. (2018a). Characteristics and aging of traffic-derived particles in a highway tunnel at a coastal city in southern China, *Science of the Total Environment*, *619-620*, 1385-1393.

Hou, C., Shao, L., Zhao, C., Wang, J., Liu, J., and Geng, C. (2018b). Characterization of coal burning-derived individual particles emitted from an experimental domestic stove, *Journal of Environmental Sciences*, *71*(9), S1001074217320119.

Huang, G., Cheng, T., Zhang, R., Tao, J., Leng, C., Zhang, Y., Zha, S., Zhang, D., Xiang, L., and Xu, C. (2014a). Optical properties and chemical composition of PM2.5 in Shanghai in the spring of 2012, *Particuology*, *13*(2), 52-59.

Huang, R. J., Zhang, Y., Bozzetti, C., Ho, K. F., Cao, J., Han, Y., Daellenbach, K. R., Slowik, J. G., Platt, S. M., and Canonaco, F. (2014b). High secondary aerosol contribution to particulate pollution during haze events in China, *Nature*, *514*(7521), 218-222.

Kim, S. E., Honda, Y., Hashizume, M., Kan, H., Lim, Y. H., Lee, H., Kim, C. T., Yi, S. M., and Kim, H. (2017). Seasonal analysis of the short-term effects of air pollution on daily mortality in Northeast Asia, *Science of the Total Environment*, *576*, 850-857.

Lan, Z., Zhang, B., Huang, X., Qiao, Z., Yuan, J., Zeng, L., Hu, M., and He, L. (2018). Source apportionment of PM_(2.5) light extinction in an urban atmosphere in China, *Journal of Environmental Sciences*, *63*(1), 277-284.

Laskin, A., Gilles, M. K., Knopf, D. A., Wang, B., and China, S. (2016). Progress in the analysis of complex atmospheric particles. *Annual Review of Analytical Chemistry, 9(1)*:117-143

Li, G., Bei, N., Cao, J., Huang, R., Wu, J., Tian, F., Wang, Y., Liu, S., Qiang, Z., and Tie, X. (2017a). A possible pathway for rapid growth of sulfate during haze days in China, *Atmospheric Chemistry & Physics*, *17*(5), 1-43.

Li, J., Shao, L., Chang, L., Xing, J., Wang, W., Li, W., and Zhang, D. (2018). Physicochemical characteristics and possible sources of individual mineral particles in a dust storm episode in Beijing, China, *Atmosphere*, *9*(7), 269. https://doi.org/10.3390/atmos9070269

Li, R., Hu, Y., Li, L., Fu, H., and Chen, J. (2017b). Real-time aerosol optical properties, morphology and mixing states under clear, haze and fog episodes in the summer of urban Beijing, *Atmospheric Chemistry & Physics*, *17*(8), 1-40.

Li, W., and Shao, L. (2009). Transmission electron microscopy study of aerosol particles from the brown hazes in northern China, *Journal of Geophysical Research Atmospheres*, *114*, D09302, doi:10.1029/2008JD011285.

Li, W., Shao, L., Shi, Z., Chen, J., Yang, L., Yuan, Q., Yan, C., Zhang, X., Wang, Y., and Sun, J. (2014). Mixing state and hygroscopicity of dust and haze particles before leaving Asian continent, *Journal of Geophysical Research Atmospheres*, *119*(2), 1044-1059.

Li, W., Shao L., Zhang, D., Ro, C. U., Hu, M., Bi, X., Hong, G., Matsuki, A., Niu, H., and Chen, J. (2016a). A review of single aerosol particle studies in the atmosphere of East Asia: morphology, mixing state, source, and heterogeneous reactions, *Journal of Cleaner Production*, *112*, 1330-1349.

Li, W., Sun, J., Xu, L., Shi, Z., Riemer, N., Sun, Y., Fu, P., Zhang. J., Lin, Y., and Wang, X. (2016b). A conceptual framework for mixing structures in individual aerosol particles, *Journal of Geophysical Research*, *121*(22).

Li, W., Shao, L., Wang, W., Li, H., Wang, X., Li, Y., Li, W., Jones, T.P., Zhang, D. (2020). Air quality improvement in response to intensified control strategies in Beijing during 2013–2019, *Science of The Total Environment,* 140776, https://doi.org/10.1016/j.scitotenv.2020.140776.

Liu, L., Kong, S., Zhang, Y., Wang, Y., Xu, L., Yan, Q., Lingaswamy, A. P., Shi, Z., Lv, S., and Niu, H. (2017). Morphology, composition, and mixing state of primary particles from combustion sources - crop residue, wood, and solid waste, *Sci Rep*, *7*(1), 5047.

Liu, Y., Jia, R., Dai, T., Xie, Y., and Shi, G. (2014). A review of aerosol optical properties and radiative effects, *Journal of Meteorological Research*, *28*(6), 1003-1028.

Lu, Y., Wang, Y., Zuo, J., Jiang, H., Huang, D., and Rameezdeen, R. (2018). Characteristics of public concern on haze in China and its relationship with air quality in urban areas, *Science of the Total Environment*, *s 637–638*, 1597-1606.

MEPC (Ministry of Environmental Protection of China), 2017. Action Plan for Comprehensive Control of Atmospheric Pollution in Autumn and Winter of Beijing-Tianjin-Hebei region in 2017–2018. available at. http://www.mee.gov.cn/gkml/hbb/bwj/201708/t20170824_420330.htm. (in Chinese).

Niu, H., Hu, W., Pian, W., Fan, J., and Wang, J. (2015). Evolution of atmospheric aerosol particles during a pollution accumulation process: a case study, *World Journal of Engineering*, *12*(1), 51-60.

Niu, H., Hu, W., Zhang, D., Wu, Z., and Guo, S. (2016). Variations of fine particle physiochemical properties during a heavy haze episode in the winter of Beijing, *Science of the Total Environment, 571,* 103–109.

Okada, K., Yu, Q., and Kai, K. (2005). Elemental composition and mixing properties of atmospheric mineral particles collected in Hohhot, China, *Atmospheric Research*, *73*(1), 45-67.

Peng, Z., Wang, Q., Kan, H., Chen, R., and Wang, W. (2017). Effects of ambient temperature on daily hospital admissions for mental disorders in Shanghai, China: A time-series analysis, *Science of the Total Environment*, *590*, 281-286.

Posfai, M., and Buseck, P. R. (2010), Nature and climate effects of individual tropospheric aerosol particles, *Annu. Rev. Earth Planet. Sci., 38(1)*, 17–43.

Qi, Y., Li, W., and Zhang, H. (2014). Local and inter-regional contributions to PM 2.5 nitrate and sulfate in China, *Atmospheric Environment*, *94*, 582-592.

Rao, X., Zhang, H., Ma, X., and Cao, Y. (2015). Cause Analysis on the Extreme Fog-haze Event in East China in January 2013, *Meteorological & Environmental Research*(7), 10-16.

Shao, L., Hu, Y., Shen, R., Schäfer, K., Wang, J., Wang, J., Schnelle-Kreis, J., Zimmermann, R., Bérubé, K., and Suppan, P. (2017a). Seasonal variation of particle-induced oxidative potential of airborne particulate matter in Beijing, *Science of the Total Environment*, *579*, 1152-1160.

Shao, L., Hu, Y., Fan, J., Wang, J., Wang, J., and Ma, J. (2017b). Physicochemical Characteristics of aerosol particles in the tibetan Plateau: Insights from TEM-EDX analysis, *Journal of Nanoscience & Nanotechnology*, *17*(9), 6899-6908.

Song, X., Shao, L., Zheng, Q., and Yang, S. (2014). Mineralogical and geochemical composition of particulate matter (PM10) in coal and non-coal industrial cities of Henan Province, North China, *Atmospheric Research*, *143*(24), 462-472.

Sun, Y., Jiang, Q., Wang, Z., Fu, P., Li, J., Yang, T., Yin, Y. (2014). Investigation of the sources and evolution processes of severe haze pollution in Beijing in January 2013. *Journal of Geophysical Research: Atmospheres, 119(7)*:4380-4398.

Sun, J., Liu, L., Xu, L., Wang, Y., Wu, Z., Hu, M., Shi, Z., Li, Y., Zhang, X., and Chen, J. (2018). Key role of nitrate in phase transitions of urban particles: implications of important reactive surfaces for secondary aerosol formation, *Journal of Geophysical Research: Atmospheres*, *123*(16).

The State Council of China, 2013. Air Pollution Prevention and Control Action Plan. http://www.gov.cn/zwgk/2013-09/12/content_2486773.htm (accessed 12 September 2013).

Tian, P., Wang, G., Zhang, R., Wu, Y., and Yan, P. (2015). Impacts of aerosol chemical compositions on optical properties in urban Beijing, China, *Particuology*, *18*(1), 155-164.

UN Environment. (2019). A Review of 20 Years' Air Pollution Control in Beijing. United Nations Environment Programme, Nairobi, Kenya.

Wang Z, Li J, Wang Z, Yang, W.Y., Tang X., Ge, B., et al. (2014a). Modeling study of regional severe hazes over mid-eastern China in January 2013 and its implications on pollution prevention and control, *Science China Earth Sciences, 57(1)*:3-13.

Wang, Y., Yao, L., Wang, L., Liu, Z., Ji, D., Tang, G., Zhang, J., Sun, Y., Hu, B., Xin J. (2014b). Mechanism for the formation of the January 2013 heavy haze pollution episode over central and eastern China, *Science China Earth Sciences, 57(1)*:14-25

Wang, G., Zhang, R., Gomez, M. E., Yang, L., Levy, Z. M., Hu, M., Lin, Y., Peng, J., Guo, S., and Meng, J. (2016). Persistent sulfate formation from London Fog to Chinese haze, *Proceedings of the National Academy of Sciences of the United States of America*, *48*(113), 13630-13635.

Wang, W., Shao, L., Guo, M., Hou, C., Xing, J., Wu, F. (2017). Physicochemical properties of individual airborne particles in Beijing during pollution periods. *Aerosol and Air Quality Research, 17*, 3209–3219, doi: 10.4209/aaqr.2017.03.0116

Wang, W., Shao, L., Li, J., Chang, L., Zhang, D., Zhang, C., and Jiang, J. (2019), Characteristics of individual particles emitted from an experimental burning chamber with coal from the lung cancer area of Xuanwei, China, *Aerosol and Air Quality Research*, *19*, 355-363.

Wang, X., Shen, X., Sun, J., Zhang, X., Wang, Y., Zhang, Y., Wang, P., Xia, C., Qi, X., Zhong, J. (2018). Size-resolved hygroscopic behavior of atmospheric aerosols during heavy aerosol pollution episodes in Beijing in December 2016. *Atmospheric Environment, 194*, 188–197. doi:10.1016/j.atmosenv.2018.09.041.

Xing, J., Shao, L., Zhang, W., Peng, J., Wang, W., Hou, C., Shuai, S., Hu, M., and Zhang, D. (2018). Morphology and composition of particles emitted from a port fuel injection gasoline vehicle under real-world driving test cycles, *Journal of Environmental Sciences*, *76*(2), S1001074218305977-.

Xing, J., Shao, L., Zheng, R., Peng, J., Wang, W., Guo, Q., Wang, Y., Qin, Y., Shuai, S., and Hu, M. (2017). Individual particles emitted from gasoline engines: Impact of engine types, engine loads and fuel components, *Journal of Cleaner Production*, *149*,

461-471.

Xing, J., Shao, L, Zhang, W., Peng, J., Wang, W., Shuai, S., Hu, M., and Zhang, D. (2020). Morphology and size of the particles emitted from a gasoline-direct-injection-engine vehicle and their ageing in an environmental chamber, *Atmospheric Chemistry & Physics*, 20, 2781–2794. https://doi.org/10.5194/acp-20-2781-2020

Yuan, Q., Li, W., Zhou, S., Yang, L., Chi, J., Sui, X., and Wang W. (2015). Integrated evaluation of aerosols during haze-fog episodes at one regional background site in North China Plain, *Atmospheric Research*, *156*, 102-110.

Zeng, X. W., Vivian, E., Mohammed, K., Jakhar, S., Vaughn, M., Huang, J., Zelicoff A., Xaverius P., Bai Z., and Lin S. (2016). Long-term ambient air pollution and lung function impairment in Chinese children from a high air pollution range area: The Seven Northeastern Cities (SNEC) study, *Atmospheric Environment*, *138*, 144-151.

Zhang, Q., Quan, J., Tie, X., Li, X., Liu, Q., Gao, Y., and Zhao, D. (2015). Effects of meteorology and secondary particle formation on visibility during heavy haze events in Beijing, China, *Science of the Total Environment*, *502*, 578-584.

Zhang, Y., Cai, J., Wang, S., He, K., and Zheng, M. (2017). Review of receptor-based source apportionment research of fine particulate matter and its challenges in China, *Science of the Total Environment*, *586*, 917-929.

Zhong, J., Zhang, X., Wang, Y., SUN J., ZHANG Y., WANG, J. et al. (2017). Relative contributions of boundary-layer meteorological factors to the explosive growth of PM2.5 during the red-alert heavy pollution episodes in Beijing in December 2016. *Journal of Meteorological Research 31,* 809–819. https://doi.org/10.1007/s13351-017-7088-0.

Zieger, P., Väisänen, O., Corbin, J. C., Partridge, D. G., Bastelberger, S., Mousavi-Fard, M., Rosati, B., Gysel, M., Krieger, U. K., and Leck, C. (2017). Revising the hygroscopicity of inorganic sea salt particles, *Nature Communications*, *8*, 15883.

**Figures:**



**Tables:**

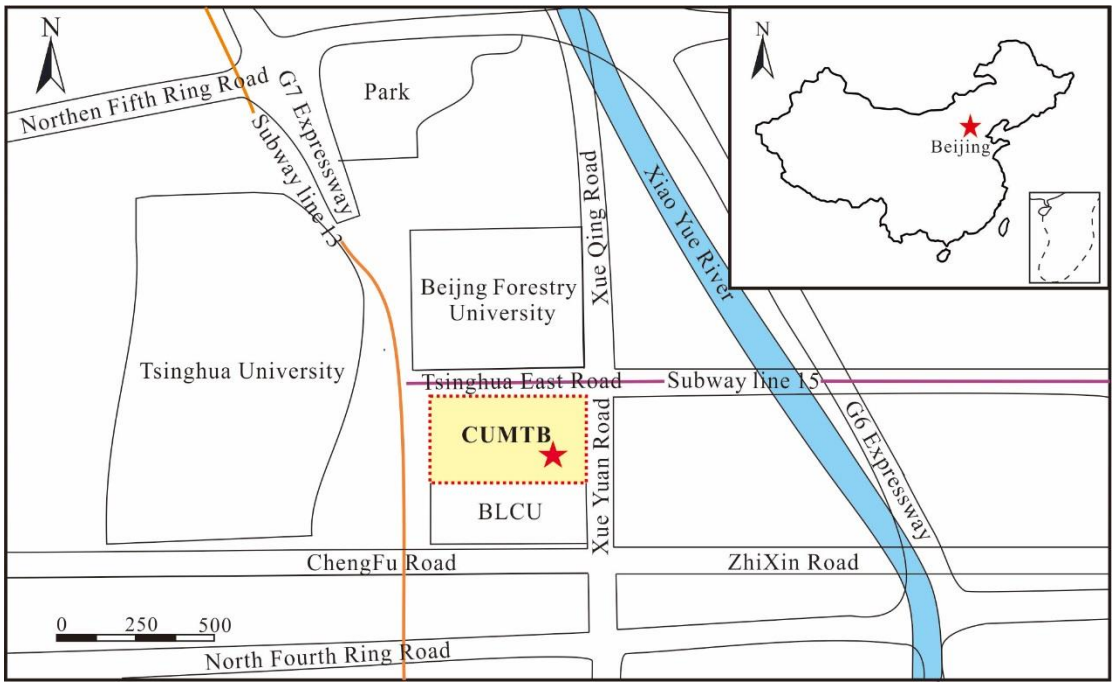


Figure 1 Location of the sampling site marked with star and the surrounding environments

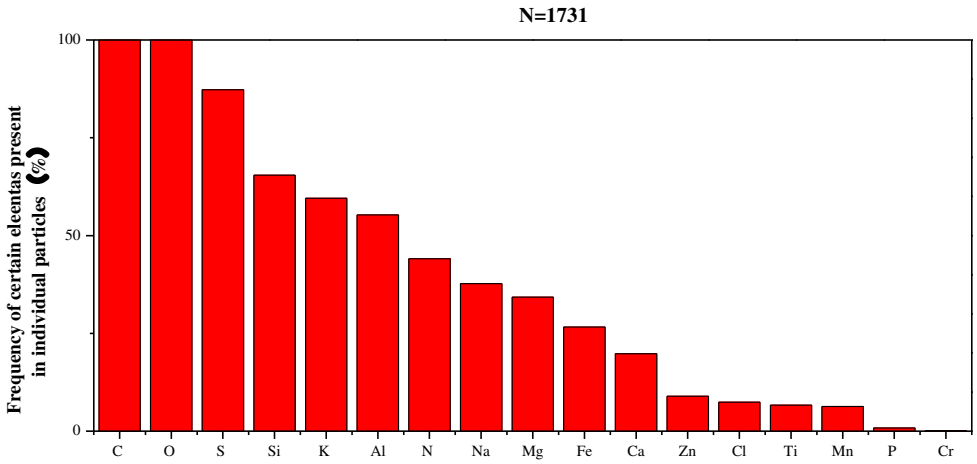


Figure 2 Overall detection frequencies of elements in the individual particles after the Action Plan

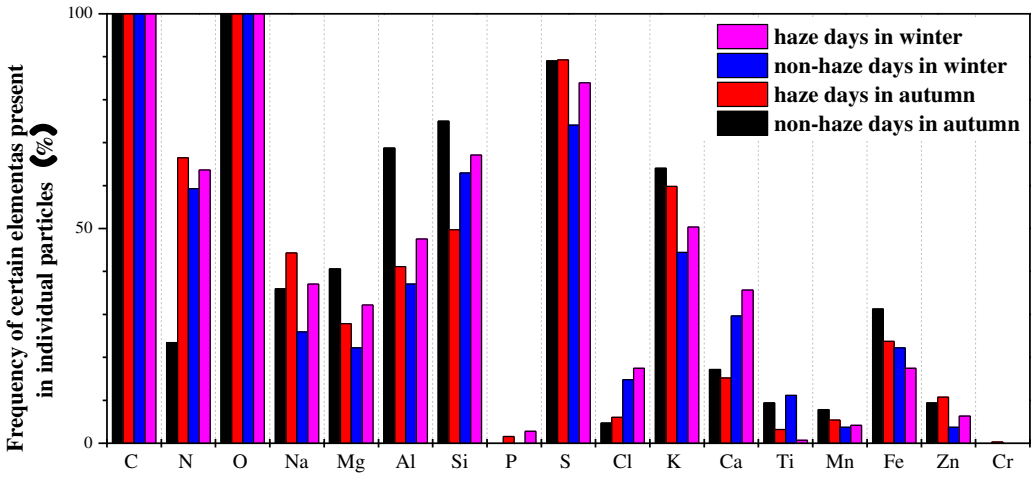


Figure 3 The detection frequencies of elements in the individual particles under different meteorological conditions in autumn and winter during the Action Plan

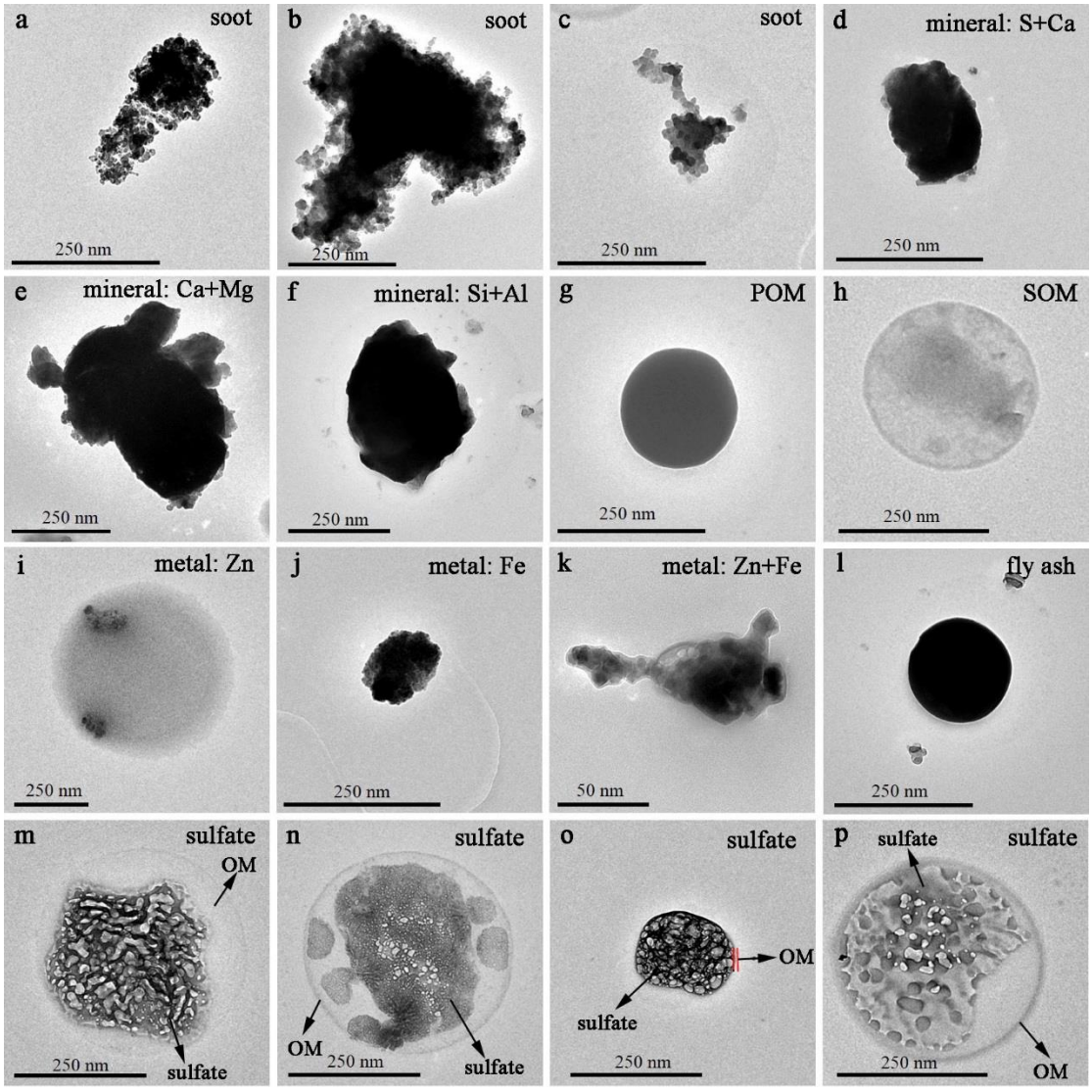


Figure 4 TEM images showing individual particle types in haze and non-haze days in autumn and winter in Beijing after the Action Plan

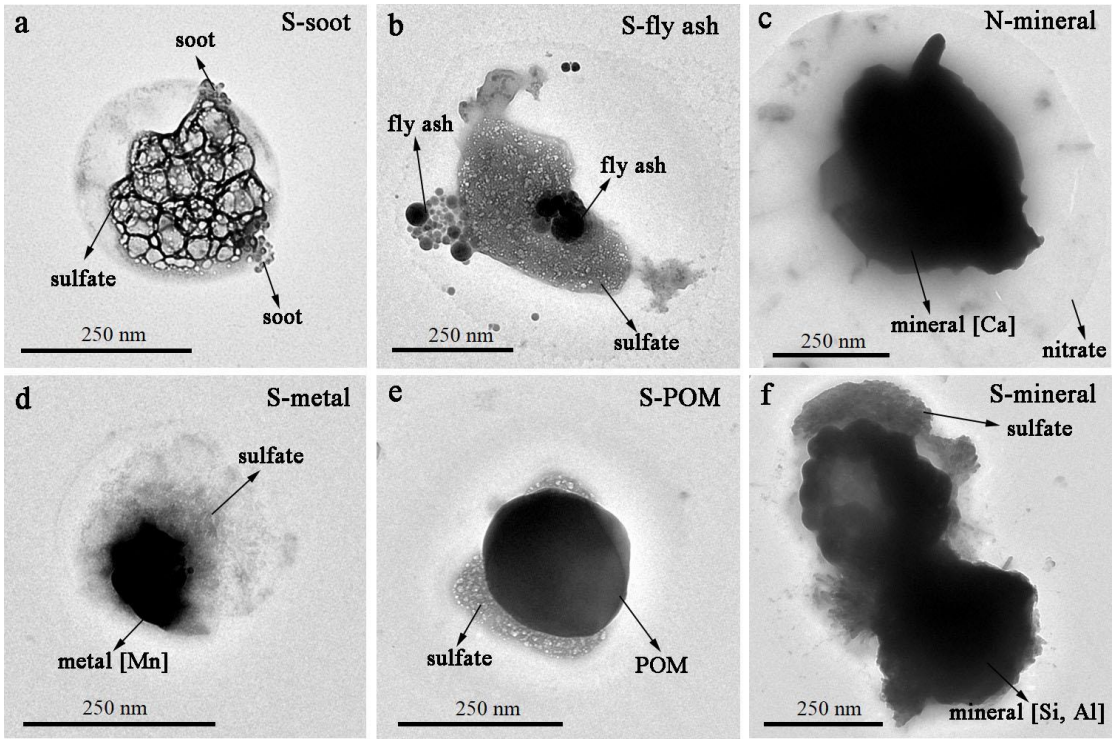


Figure 5 TEM images showing morphology of mixture particles collected in non-haze days and haze days in autumn and winter in Beijing after the Action Plan. (a) S-soot mixture, represented by sulfate aggregates internally mixed with core-shell sulfate particle, (b) S-fly ash mixture, represented by fly ash internally mixed with sulfate particle with secondary organic coating, (c) N-mineral mixture, represented by mineral particle with nitrate coating, (d) S-metal mixture, represented by metal particle internally mixed with sulfate particle, (e) S-POM mixture, represented by primary organic particle internally mixed with sulfate particle, (f) S-mineral mixture, represented by mineral particle internally mixed with sulfate particle.

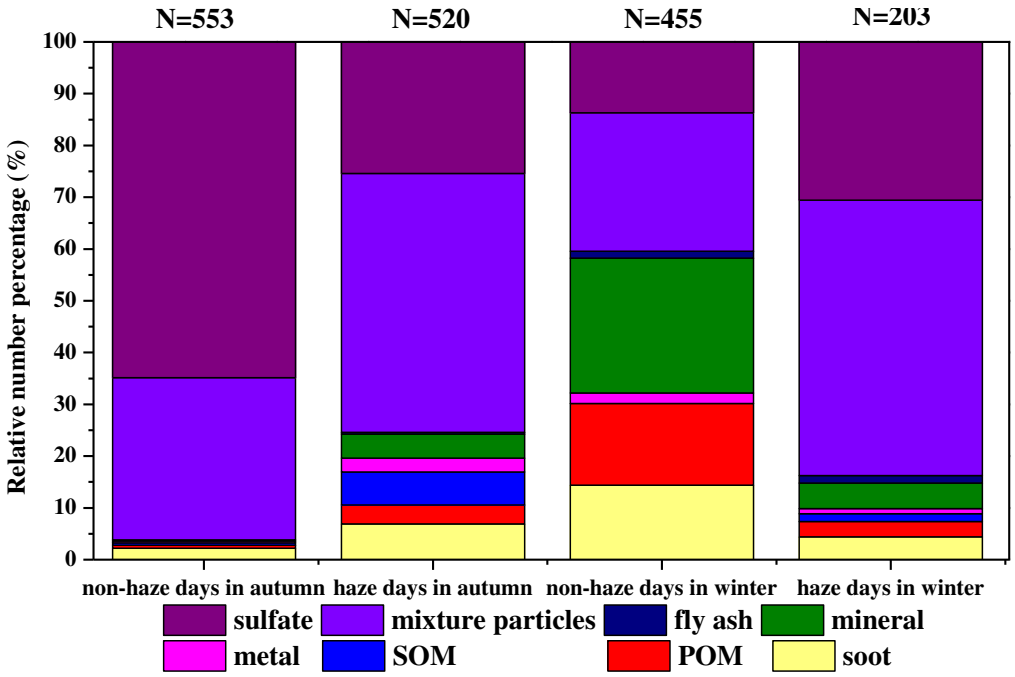


Figure 6 The relative abundance of individual particles in non-haze days and haze days in autumn and winter during the Action Plan

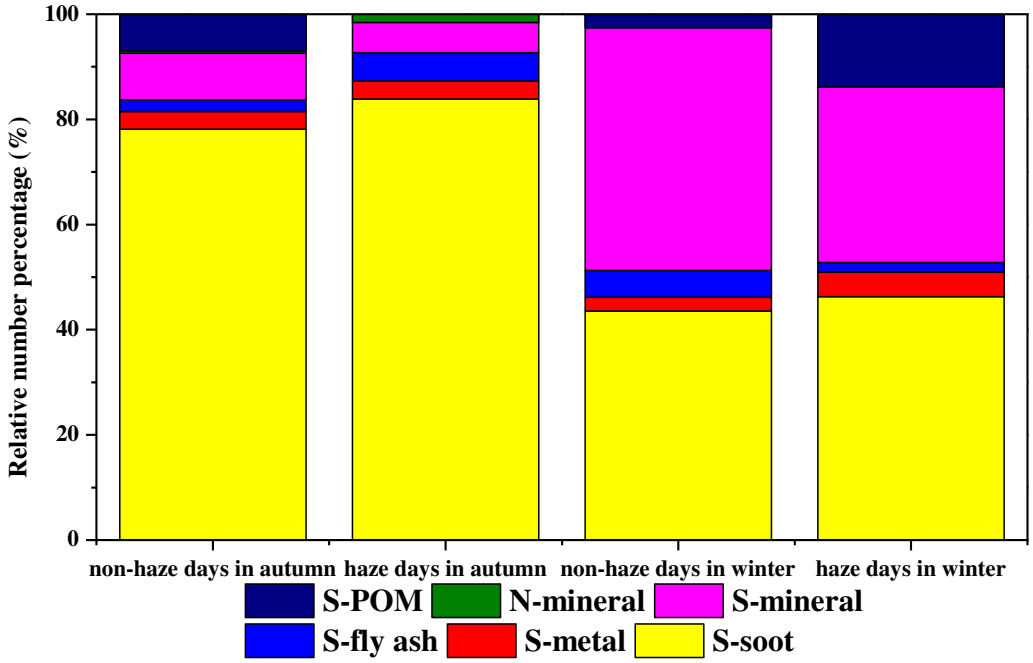


Figure 7 The relative abundance of mixture particles in non-haze days and haze days in autumn and winter after the Action Plan

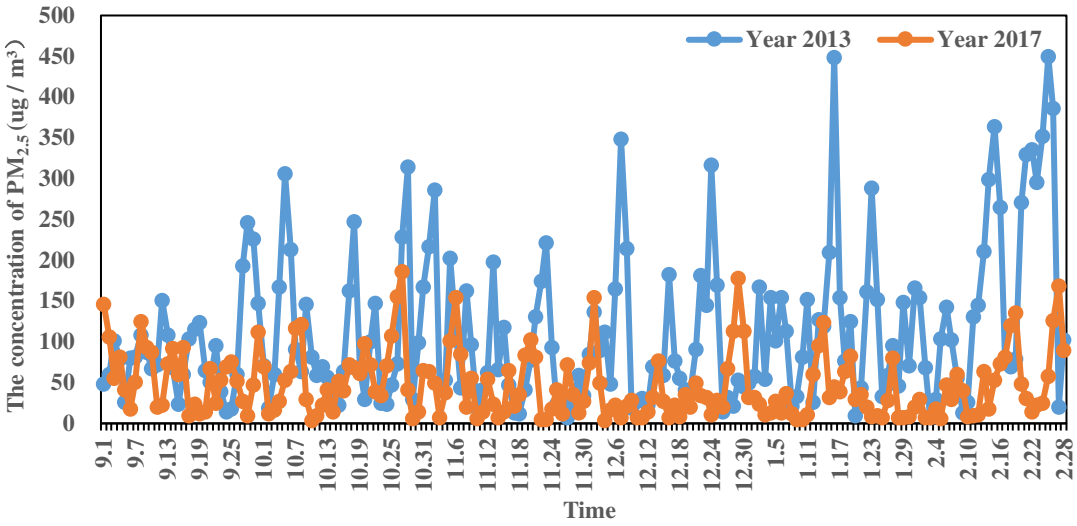


Figure 8 The concentration of $PM_{2.5}$ before and after the Action Plan in autumn and winter

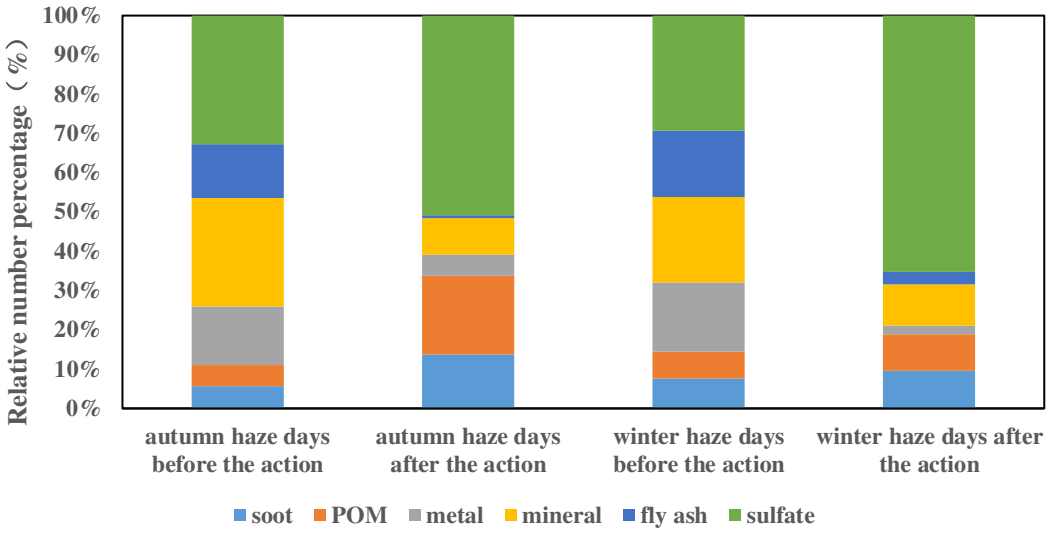


Figure 9　Relative number percentages of individual particles collected in the haze days before and after the Action Plan in autumn and winter

Table 1 Sample information for individual particle analysis of $PM_{2.5}$ in Beiijng after the Action Plan

| Meteorological conditions | Sample No. | Sampling time (BST) | Sampling season | Sampling duration (s) | T (℃) | RH (%) | P (hPa) | Concentration of $PM_{2.5}$ (μg/m³) |
|---|---|---|---|---|---|---|---|---|
| haze | A | 2017/9/14 8:15 | autumn | 20s | 25.2 | 72 | 1010.1 | 143 |
| haze | B | 2017/10/27 10:04 | autumn | 5s | 17.9 | 63.8 | 1010.9 | 170 |
| haze | C | 2017/11/21 8:05 | winter | 10s | 2.5 | 47.5 | 1013.3 | 149 |
| haze | D | 2017/11/21 18:32 | winter | 15s | 10.3 | 17.9 | 1011.9 | 189 |
| haze | E | 2017/12/29 8:38 | winter | 20s | -1 | 65.6 | 1022.8 | 127 |
| haze | F | 2018/1/19 21:48 | winter | 25s | 4.8 | 33.5 | 1015.5 | 170 |
| non-haze | G | 2017/10/23 9:56 | autumn | 50s | 18.9 | 48.8 | 1019 | 28 |
| non -haze | H | 2017/10/24 9:58 | autumn | 60s | 18.3 | 48.6 | 1018.9 | 38 |
| non-haze | I | 2018/1/12 11:32 | winter | 85s | 6.8 | 20.7 | 1022.4 | 36 |

Table 2 The types of individual particles in $PM_{2.5}$ based on TEM-EDX

| Individual particles | | Major element | Morphologies | Major sources |
|---|---|---|---|---|
| Soot aggregates | | C, O, and minor Si, K | Chain-like, cluster-like, and compact-like morphologies | Emission of vehicles burning fossil fuel |
| Mineral particles | | Si, Al, Ca, Mg, K, and Fe | Irregular morphologies | Road dust, construction dust, and desert |
| Organic particles | Primary organic particles (tar balls) | C and O | Spherical and near-spherical morphologies | Fossil fuel and biomass burning |
| | Secondary organic particles | C, O, and S | Irregular morphologies | Secondary conversion of volatile organic compounds (VOCs) |
| Metal particles | | Zn, Fe, Pb, Mn, and minor Cr | Spherical and irregular morphologies | The coal-fired power plant, heavy industries, and tire abrasion |
| Fly ashes | | Si, Al, Fe and minor Na, K | Spherical morphology | Coal combustion |
| Sulfate particles | | S and minor Na, K, Ca | Irregular morphologies and core-shell structure | Transformed by $SO_2$ emitted from coal combustion or vehicles |
| Mixture particles | S-soot | Sulfate internally mixed with soot, metal, fly ash, mineral, and primary organic particle | Irregular, spherical, or core-shell structure | The mixture of secondary particles and primary particles are formed by heterogeneous chemical reaction |
| | S-metal | | | |
| | S-fly ash | | | |
| | S-mineral | | | |
| | S-POM | | | |
| | N-mineral | Nitrate internally mixed with mineral | | |